Identification of a novel endocytosis-associated gene signature for prognostic prediction in lung adenocarcinoma

YIXIN ZHANG[1*], SIWEN LIANG[2*], YAN ZHANG[1], MINGHUI LIU[3] and KAI ZHANG[1]

[1]Department of Blood Transfusion, Tianjin Hospital, Tianjin 300211; [2]School of Optometry & Ophthalmology, Tianjin Medical University, Tianjin 300070; [3]Department of Lung Cancer Surgery, Tianjin Medical University General Hospital, Tianjin 300052, P.R. China

Abstract. Lung cancer is one of the most common malignant solid tumors and the leading cause of cancer-associated mortality worldwide. Endocytosis is an essential physiological activity for cells to maintain membrane homeostasis, and has been reported to serve an important role in tumorigenesis and progression. In the present study, the aim was to construct a prognostic prediction model of endocytosis-associated genes for patients with lung adenocarcinoma (LUAD). The endocytosis-associated gene signature was established using Lasso Cox regression analysis using the training set of the LUAD cohort from The Cancer Genome Atlas (TCGA) database, and verified using two datasets from the Gene Expression Omnibus (GEO) database. Kaplan-Meier survival curves were used to evaluate the effectiveness of the prognostic evaluation of patients with LUAD. Differentially expressed genes were screened in the tumor tissue of patients compared with paired paracancerous tissues. A series of candidate genes associated to the prognosis of patients with LUAD was obtained using univariate Cox's regression analysis. Using the Lasso Cox regression analysis, an appropriate risk model with 18 endocytosis-associated genes was established. A high-risk score was positively correlated with a higher tumor stage and pathologic grade. Patients with LUAD and high-risk scores had shorter survival times, increased intratumor heterogeneities and immune cell infiltration into tumor tissues, compared with those patients with LUAD and low-risk scores. The endocytosis inhibitor chloroquine could repress proliferation and increase the apoptosis of lung cancer cells. In summary, a novel endocytosis-associated gene signature was constructed using TCGA and GEO datasets. Patients with LUAD and high-risk scores, as calculated by the signature, had a poor prognosis and short survival time.

Introduction

As the malignant tumor with fast growth in incidence (28.3 per 100,000) and mortality rate (23.0 per 100,000), lung cancer poses a threat to human health (1,2). According to the histological origin, lung cancer is usually divided into small cell lung cancer (SCLC) and non-SCLC (NSCLC) (3). NSCLC is the most common pathological type of lung cancer, accounting for ~85%, including lung adenocarcinoma (40%), lung squamous cell carcinoma (25%), large cell carcinoma and other subtypes (4,5). Lung cancer prognosis is improved if it is detected and treated at an early stage. However, patients often miss the optimal treatment period due to late diagnosis and the advanced stage of the disease. Although patients receive a series of treatments, including radiotherapy and chemotherapy, targeted therapy, and immune checkpoint therapy, the prognosis is poor (6). Therefore, effective biomarkers/signatures for the early diagnosis of lung cancer are important for patients with lung cancer.

Endocytosis is an important physiological function in cell activity that engulfs extracellular substances into cells in a membrane-dependent manner, maintaining cell-cell interactions via molecule exchange (7). Endocytosis mainly includes the ingestion of two types of molecules, namely large particles and small vesicles. In cancer cells, receptor-mediated and vesicle-dependent endocytosis not only provides sufficient energy and substances for promoting the malignant progression of tumors and activates important signaling pathways for tumorigenesis, but also affects the activation state of the intracellular signaling pathway for cell-cell communication and acquired chemoresistance (8,9). Emerging evidence indicated that endocytosis contributed to signaling via its 'canonical' and 'noncanonical' mechanisms (10). For example, inhibition of endocytosis blocked H-Ras-mediated cell differentiation and Raf-1 activation (11). In addition, tumor cells

Correspondence to: Dr Kai Zhang, Department of Blood Transfusion, Tianjin Hospital, 406 Jiefang South Road, Tianjin 300211, P.R. China
E-mail: tjyy_zhangkai@yeah.net

Dr Minghui Liu, Department of Lung Cancer Surgery, Tianjin Medical University General Hospital, 154 Anshan Road, Tianjin 300052, P.R. China
E-mail: liuminghui2012@hotmail.com

*Contributed equally

can drive a microenvironment suitable for tumorigenesis and metastasis via interaction with surrounding cells including stromal, immune and vascular cells. For example, clathrin light chain b, the essential isoform of the clathrin receptor in clathrin-mediated endocytosis, enhances the epidermal growth factor receptor (EGFR)/AKT/glycogen synthase kinase 3β (GSK-3β) signal transduction, contributing to tumor progression and metastasis in lung cancer (12). Therapeutic strategies targeting endocytosis have been demonstrated to have the potential to inhibit tumor growth and sensitize lung cancer to conventional chemotherapeutic drugs (12-14). For example, the clathrin-mediated endocytosis inhibitor PAO combined with gefitinib resulted in tumor regression and increased apoptosis in NSCLC (12). The aforementioned *in vitro* studies, carried out using lung cancer cell lines such as H358, Calu-3, SNU-1327, H1299, HCC4017, H441 and H522, and *in vivo* experiments involving xenografts established in nude mice, revealed that inhibition of clathrin-mediated endocytosis decreased the malignant progression and enhanced the anti-tumor effect of tyrosine kinase inhibitors (TKIs) against lung cancer (15-18). However, studies focusing on lung cancer prognostic prediction models based on endocytosis-associated genes have not been reported.

In the present study, the differentially expressed genes (DEGs) in tumor samples compared with paracancerous tissues from the lung adenocarcinoma (LUAD) cohort in The Cancer Genome Atlas (TCGA) database were screened, and these DEGs were integrated with endocytosis-associated genes. To investigate the effect of these endocytosis-associated genes on the prognosis prediction of patients with LUAD, a novel endocytosis-associated gene signature was constructed, and its prognostic value was examined using TCGA and Gene Expression Omnibus (GEO) databases. Based on the experimental verification of the expression patterns of these genes *in vitro*, the endocytosis inhibitor chloroquine (CQ) was used to investigate changes in the expression of the aforementioned genes and their anti-tumor effect.

Materials and methods

Acquisition of LUAD transcriptome data in TCGA and GEO databases. The RNA sequencing data of LUAD in TCGA database were downloaded from the UCSC Xena online server (https://xenabrowser.net/). The gene expression matrices of GSE30219 and GSE31210 were obtained from the GEO database (https://www.ncbi.nlm.nih.gov/geo/). Data were transformed as follows: $i=2^i-1$ for subsequent analysis.

Collection of endocytosis-associated genes. Endocytosis-associated genes were collected from the Gene Ontology (GO) (https://geneontology.org/), Kyoto Encyclopedia of Genes and Genomes (https://www.kegg.jp/) database and the Reactome Knowledgebase (www.reactome.org). The search term 'endocytosis' was used. In total, 24 gene sets were obtained, and were intersected for endocytosis-associated genes.

DEG analysis in TCGA-LUAD cohort. Based on the clinical information of the LUAD cohort from TCGA, the RNA sequencing data of 60 tumor and paired paracancerous tissues were used for differential expression analysis via the DESeq2

R package (version 1.30.0) (19). DEGs were identified using the criteria of absolute value of Log fold-change (FC) >1.2, adjusted P≤0.05 and visualized as volcano plots. The intersection between DEGs and endocytosis-associated genes was used as a candidate for univariant Cox regression analysis.

Cox regression and Kaplan-Meier survival analyses. Cox regression and Kaplan-Meier survival analyses were performed against candidate genes using the Survival R package (version 3.5-5; https://github.com/therneau/survival) to measure the association between expression level and overall survival in TCGA-LUAD, GSE30219 and GSE31210 cohorts. Genes with significant P-values were selected for Lasso Cox regression analysis using the glmnet R package (version 4.1-3; https://glmnet.stanford.edu/), and the refined prognostic model was constructed. The risk scores of each patient were calculated using the following formula: $RiskScore=\Sigma exp_i \times \beta_i$, where exp_i was the expression of gene i and β_i referred to the coefficient calculated by univariate Cox regression analysis of gene i.

GO analysis. Metascape (https://metascape.org) is an online tool for gene function annotation analysis, and it was used to analyze the GO enrichment of the 18 genes in the novel signature. Results were visualized as network plots.

Detection of tumor purity and immune cell composition. The tumor purities of TCGA-LUAD, GSE30219 and GSE31210 cohorts were calculated using the ESTIMATE R package (version 1.0.13; https://r-forge.r-project.org/projects/estimate/) (20). Briefly, gene symbols and their corresponding expression levels were used as input data. After transformation and calculation by the 'filterCommonGenes' and 'estimateScore' functions, purity data were obtained. The Pearson's correlation coefficient was used for investigating the correlation between the riskScore and tumor purity was visualized as scatter plots.

Immune cell compositions were acquired via the CIBERSORTx (https://cibersortx.stanford.edu/) online analytical tool. By performing a series of steps to input the signature matrix file and expression file with default settings, the results were downloaded after the analysis was finished. The risk score distributions of each patient in the high and low groups were visualized as boxplots.

Cell culture. The human lung epithelial cell line BEAS-2B, and the NSCLC cell lines A549, H1299 and H1975 were obtained from the American Type Culture Collection. The NSCLC cell line PC9 was purchased from the National Collection of Authenticated Cell Cultures. The BEAS-2B and A549 cell lines were cultured in Dulbecco's Modified Eagle Medium (Thermo Fisher Scientific, Inc.) supplemented with 10% fetal bovine serum (FBS) (Gibco; Thermo Fisher Scientific, Inc.). The H1299, H1975 and PC9 cell lines were cultured in Roswell Park Memorial Institute-1640 (Thermo Fisher Scientific, Inc.) supplemented with 10% FBS. All cells were cultured at 37°C and 5% CO_2.

Cell viability assay. Cells were trypsinized to a single-cell suspension and counted. A total of 3,000 cells per well

were seeded into 96-well culture plates. CQ (cat. no. S6999; Selleck Chemicals) was dissolved in DMSO to a storage concentration of 10 mM and diluted in culture media to a working concentration of 20 μM. After either 24, 48, 72, 96 or 120 h of CQ treatment, Cell Counting Kit-8 (cat. no. CK04; Dojindo Laboratories, Inc.) reagent was added, followed by a 2 h-incubation. The OD450 absorbance was measured using a microplate reader.

5-ethynyl-2'-deoxyuridine (EdU) assay. Cultured cells were seeded into glass bottom culture dishes. After 48 h of treatment with 20 μM CQ, EdU (cat. no. C0078S; Beyotime Institute of Biotechnology.) incorporation and staining were performed according to the manufacturer's protocol. Briefly, after pretreatment with 10 μM EdU for 2 h, cells were fixed with 4% paraformaldehyde solution for 10 min at room temperature and permeated using PBS with 0.2% Triton X-100 for 10 min at room temperature. Subsequently, Azid Alexa Fluor 594 was used to label EdU, and Hoechst 33342 was employed to stain nuclei for 10 min at room temperature protected from light. Samples were imaged using a laser confocal microscope (Olympus Corporation). The proportion of EdU-positive cells was calculated by counting the EdU-positive cells and the total number of cells using ImageJ (version 1.53; National Institutes of Health).

Reverse transcription-quantitative PCR (RT-qPCR). After 48 h of 20 μM CQ treatment, total RNA was isolated from cells using TRIzol® (Invitrogen; Thermo Fisher Scientific, Inc.) reagent according to the manufacturer's protocol, and reverse-transcribed to cDNA by using the RevertAid First Strand cDNA Synthesis Kit (cat. no. K1622; Thermo Fisher Scientific, Inc.) at 42°C for 60 min, 70°C for 5 min, and then stored at 4°C. The SYBR Green Mix (cat. no. Q711; Vazyme Biotech Co., Ltd.) was used in a thermocycler instrument (QuantStudio 3; Thermo Fisher Scientific, Inc.) according to the manufacturer's instructions as follows: Predenaturation at 95°C for 5 min, followed by 40 cycles of denaturation at 95°C for 15 sec, and annealing and extension at 60°C for 30 sec. GAPDH served as the internal control. Primer sequences are summarized in Table SI. The mRNA levels were quantified using the $2^{-\Delta\Delta Cq}$ method (21).

Apoptosis assay. Cell apoptosis was stained using Annexin V-FITC apoptosis detection kit (cat. no. C1062M; Beyotime Institute of Biotechnology) according to the manufacturer's protocol. Briefly, after 48 h of 20 μM CQ treatment, total cells in the supernatant medium and on the plate, were harvested and centrifuged at 500 x g for 10 min at room temperature. Cell pellets were resuspended in PBS buffer and counted. A total of $1x10^5$ cells were centrifuged at 500 x g for 10 min at room temperature, and resuspended in binding buffer (cat. no. C1062M; Beyotime Institute of Biotechnology) containing Annexin V-FITC and propidium iodide and incubated for 15 min at room temperature in the dark. Subsequently, cell apoptosis was detected using an Agilent NovoCyte flow cytometer (Agilent Technologies, Inc.). The data were analyzed using FlowJo (version 10.6.2; FlowJo LLC).

Statistical analysis. All statistical analyses were performed using GraphPad Prism (version 8, Dotmatics) and R (version 4.0.2; https://www.r-project.org/about.html). A paired Student's t-test was used for the analysis of two paired groups, and an unpaired independent-sample Student's t-test was used for the comparison of two experimental groups. One-way analysis of variance was performed to compare ≥3 groups, and Dunnett's post hoc test was used for multiple comparisons. The Pearson's correlation coefficient was used to investigate the correlation between risk score and either stromal or immune score, or tumor purity. Statistical results are presented as mean ± standard deviation. Univariate and multivariate Cox regression analysis were used to analyze the effect of risk factors on survival. Kaplan-Meier plots were used to assess the correlation between risk score and survival. P<0.05 was considered to indicate a statistically significant difference.

Results

Identification of differentially expressed endocytosis-associated genes correlated with the survival rate of patients with LUAD. The analysis flow chart of the present study is presented in Fig. 1. First, LUAD data were downloaded from TCGA database via the UCSC XENA online server, and the transcriptome sequencing data of paired cancerous and adjacent normal samples were selected for the identification of DEGs using the DESeq2 R package. A total of 2,324 upregulated and 1,409 downregulated DEGs were identified using the filtering criteria of absolute value of LogFC >1.2 and P-adjust ≤0.05 (Table SII), and were visualized as a volcano plot (Fig. 2A). To select the DEGs correlated with the function of endocytosis, the list of DEGs and the endocytosis-associated gene set were intersected (Table SIII), and 138 candidate genes were obtained (Fig. 2B). Subsequently, a univariate Cox regression analysis was performed to evaluate the association between the expression levels of these genes and the overall survival of patients. A total of 33 genes were indicated to be significantly correlated with survival times, of which the expression levels of five genes were associated with poor prognosis, and the others were associated with a favorable prognosis (Fig. 2C and Table SIV). The expression levels of these genes in tumor tissues (n=525) and normal tissues (n=60) in the LUAD cohort from TCGA containing a total of 585 samples were compared and visualized as boxplots (Fig. 2D). Compared with the normal tissues, the expression levels of RAB27B, ATP6V0A4, LOXL2, HTR2B, SYT2, F2RL1 and IGHM were significantly increased in tumor tissues, whereas the expression levels of the other genes, excluding EREG, were significantly decreased in the tumor tissues.

Construction of a novel gene signature to predict prognosis in TCGA-LUAD cohort. Based on the aforementioned identified candidate genes, Lasso Cox regression analysis was used to screen the optimal genes to construct the refined prognostic model. The coefficient results calculated by Lasso Cox regression analysis are presented in Fig. 3A. According to the calculation of risk factors using Cox regression, and Kaplan-Meier survival analyses, a novel gene signature of 18 genes, including CFTR, RAB27B, ADRB1, DPYSL2, ATP6V0A4, EREG, SFTPD, LOXL2, HTR2B, SYT2, ALOX15, F2RL1, IL7R, PCSK9, ADRB2, GATA2, IGHM and MRC1, was involved (Fig. 3B and Table SV). The GO
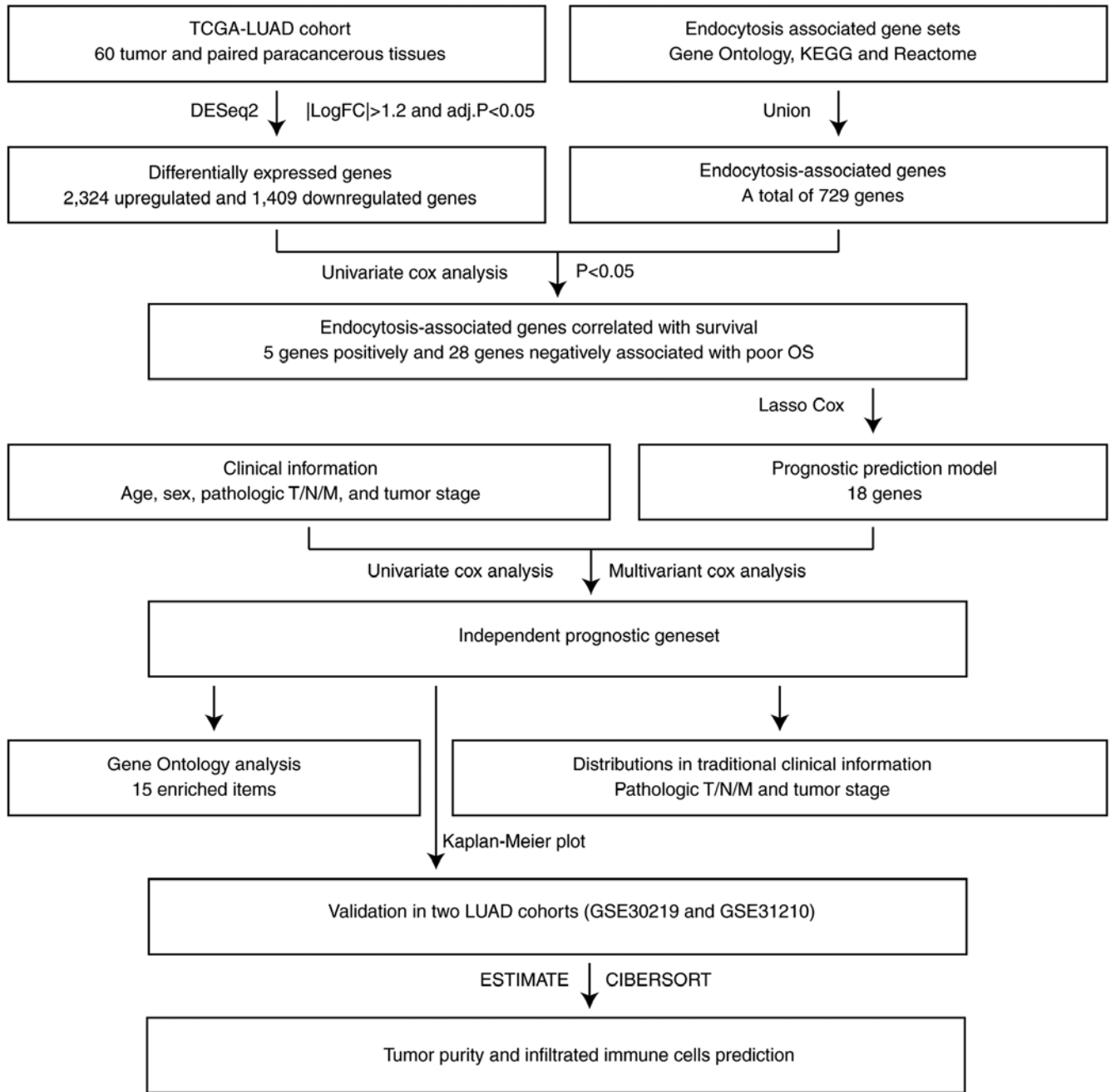
Figure 1. Scheme of the novel prognostic signature construction of lung adenocarcinoma. TCGA, The Cancer Genome Atlas; LUAD, lung adenocarcinoma; KEGG, Kyoto Encyclopedia of Genes and Genomes; OS, overall survival; T/N/M, tumor/nodal/metastasis; adj, adjusted.

analysis results revealed the enriched signaling pathways and molecular events, among which the functions associated with 'endocytosis' and 'regulation of vesicle-mediated transport' were the most significantly enriched (Fig. 3C and D).

The risk score of every patient in the LUAD cohort from TCGA was calculated based on the expression of 18 genes and the distributions in the clinical information were examined. As indicated in Fig. 3E-H, the risk score of the novel signature in different pathologic tumor (T)/nodal (N)/metastasis (M) grades and tumor stages in LUAD was significantly increased compared with that in normal tissues. As the grades or stages increased, the risk score also had an upward trend. Furthermore, univariate and multivariate Cox regression analyses were performed to evaluate the prognostic

value of the novel gene signature. As presented in Table I, the pathologic M [M1 vs. M0; hazard ratio (HR), 2.112; 95% confidence interval (CI), 1.235-3.612], pathologic N (N1 vs. N0; HR, 2.392; 95% CI, 1.700-3.365; N2 vs. N0; HR, 3.046; 95% CI, 2.084-4.452), pathologic T (T2 vs. T1; HR, 1.491; 95% CI, 1.046-2.125; T3 vs. T1; HR, 2.971; 95% CI, 1.765-4.999; T4 vs. T1; HR, 3.004; 95% CI, 1.547-5.834; TX vs. T1; HR, 4.794; 95% CI, 1.153-19.939) and tumor stage (stage II vs. stage I; HR, 2.451; 95% CI, 1.710-3.513; stage III vs. stage I; HR, 3.492; 95% CI, 2.390-5.102; stage IV vs. stage I; HR, 3.813; 95% CI, 2.203-6.599) indicated statistical significances in the univariant Cox regression analysis, whereas these were not statistically significant in the multivariant Cox regression analysis. Both univariant and multivariant Cox regression
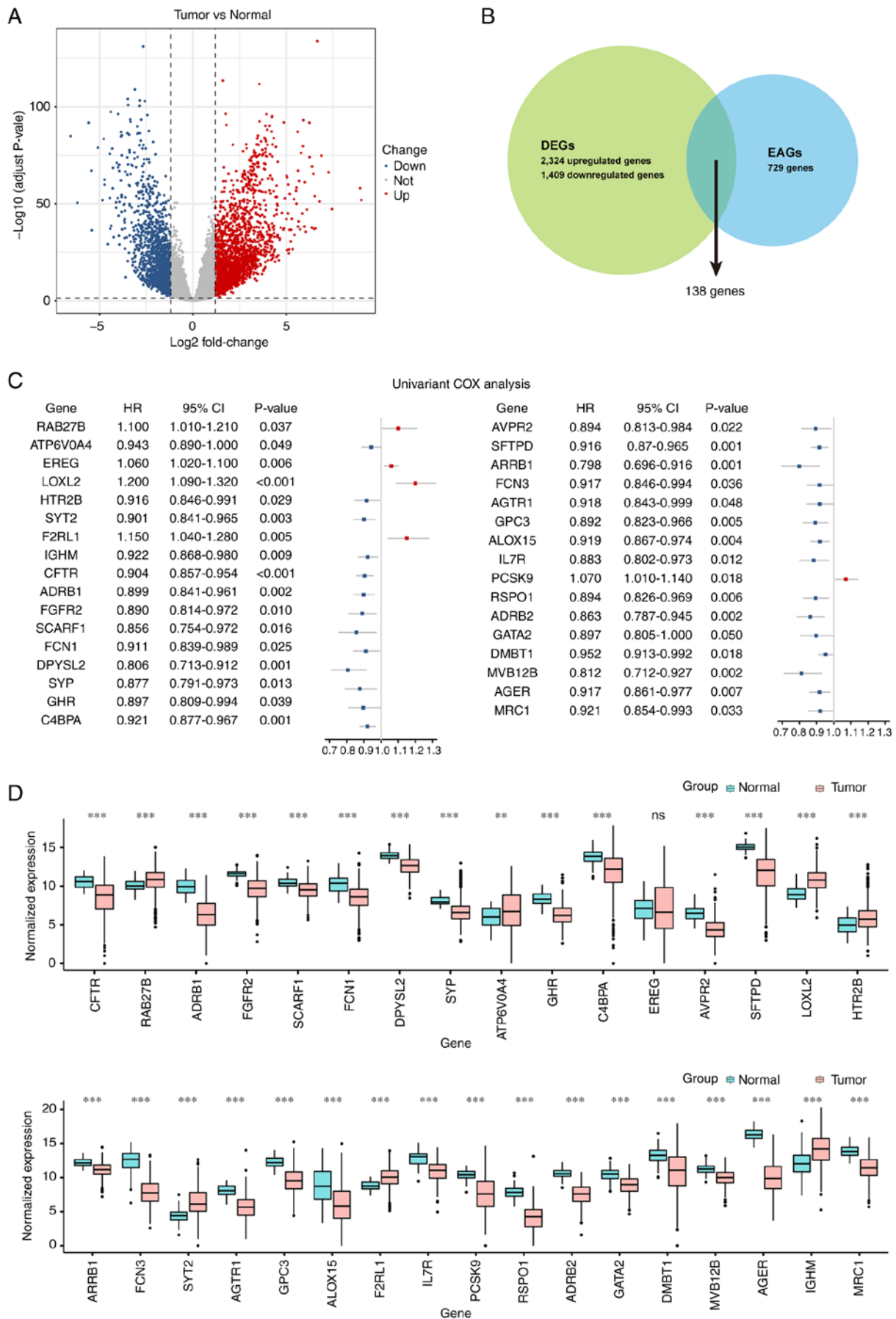
Figure 2. DEGs selected and correlated with overall survival in The Cancer Genome Atlas-LUAD cohorts. (A) Volcano plot of DEGs; red indicates upregulated genes, and blue indicates downregulated genes. (B) Intersection of DEGs and EAGs. (C) Forest plots of a total of 33 genes significantly correlated with overall survival. (D) Expression levels of 33 genes in LUAD and normal tissues were visualized as boxplots. **P<0.01; ***P<0.001. DEGs, differentially expressed genes; LUAD, lung adenocarcinoma; ns, not significant; EAGs, endocytosis-associated genes; HR, hazard ratio; CI, confidence interval.
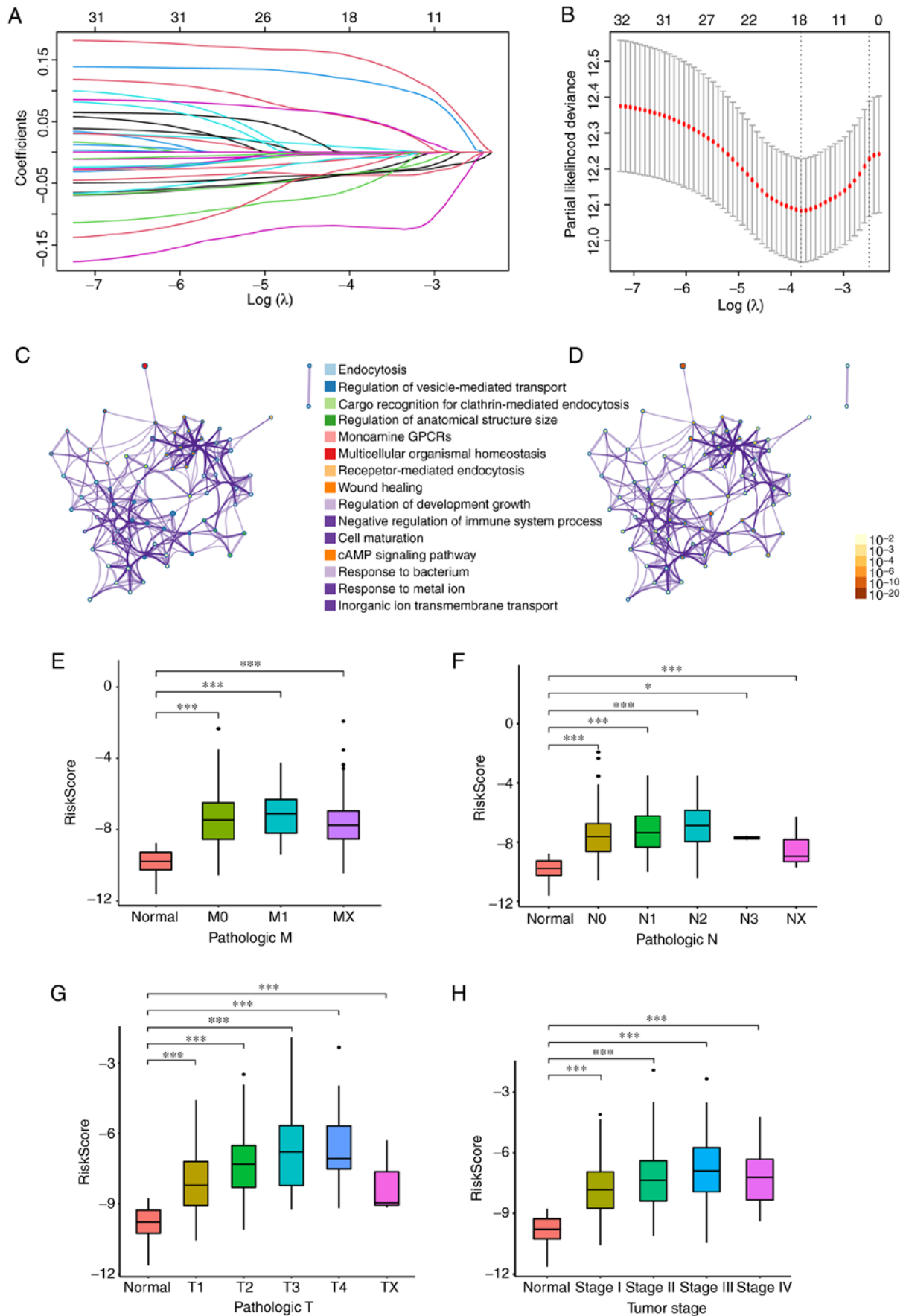
Figure 3. Novel gene signature construction and correlation between risk score and clinical information. (A) Lasso Cox regression analysis profile of 33 candidate genes. (B) Selection of the optimal gene combination using Lasso Cox regression analysis. Partial likelihood deviance against log (λ) was visualized as a dot plot. The minimal value of λ was used to select the optimal gene combination. (C and D) Network plots reveal the enriched Gene Ontology functions and P-value against key genes in the novel signature. The distributions of risk scores in different pathologic (E) M, (F) N or (G) T and (H) tumor stages were visualized as box plots. *P<0.05, ***P<0.001. M, metastatic; N, nodal; T, tumor; GPCRs, G protein-coupled receptors.

Table I. Cox regression analysis in The Cancer Genome Atlas-lung adenocarcinoma cohort.

Characteristics	Total, n	Univariant			Multivariant		
		HR	95% CI	P-value	HR	95% CI	P-value
Age, years	526	1.007	0.992-1.022	3.521×10^{-1a}	1.014	0.998-1.030	8.802×10^{-2a}
Sex							
Male	244	Reference			Reference		
Female	282	0.958	0.717-1.279	7.694×10^{-1a}	1.101	0.808-1.500	5.412×10^{-1a}
Pathologic M							
M0	354	Reference			Reference		
M1	25	2.112	1.235-3.612	6.305×10^{-3b}	0.233	0.014-3.910	3.111×10^{-1a}
MX	142	0.854	0.596-1.222	3.879×10^{-1a}	0.923	0.637-1.340	6.726×10^{-1a}
Pathologic N							
N0	341	Reference			Reference		
N1	95	2.392	1.700-3.365	5.556×10^{-7c}	1.583	0.878-2.850	1.263×10^{-1a}
N2	74	3.046	2.084-4.452	8.752×10^{-9c}	1.212	0.510-2.880	6.635×10^{-1a}
N3	2	0.000	0.000-Infinite	9.943×10^{-1a}	0.000	0.000-Infinite	9.920×10^{-1a}
NX	13	1.417	0.519-3.868	4.959×10^{-1a}	1.392	0.337-5.750	6.474×10^{-1a}
Pathologic T							
T1	172	Reference			Reference		
T2	284	1.491	1.046-2.125	2.705×10^{-2b}	1.001	0.683-1.470	9.973×10^{-1a}
T3	48	2.971	1.765-4.999	4.124×10^{-5c}	1.397	0.723-2.700	3.198×10^{-1a}
T4	19	3.004	1.547-5.834	1.163×10^{-3b}	0.844	0.378-1.880	6.789×10^{-1a}
TX	3	4.794	1.153-19.939	3.113×10^{-2b}	0.936	0.076-11.560	9.587×10^{-1a}
Tumor stage							
Stage I	286	Reference			Reference		
Stage II	122	2.451	1.710-3.513	1.050×10^{-6c}	1.372	0.734-2.560	3.217×10^{-1a}
Stage III	84	3.492	2.390-5.102	1.030×10^{-0c}	2.291	0.884-5.940	8.810×10^{-2a}
Stage IV	26	3.813	2.203-6.599	1.738×10^{-6c}	11.619	0.632-213.470	9.865×10^{-2a}
RiskScore	526	1.476	1.336-1.630	2.072×10^{-14c}	1.418	1.272-1.580	3.394×10^{-10c}

M, metastasis; N, nodal; T, tumor; HR, hazard ratio; CI, confidence interval. [a]$P \geq 0.05$; [b]$P < 0.05$; [c]$P < 0.01$.

analyses of the risk score of the novel gene signature exhibited poor survival for patient prognosis (univariant; HR, 1.476; 95% CI, 1.336-1.630; multivariant; HR, 1.418, 95% CI, 1.272-1.580), demonstrating that this novel gene signature could be an independent prognostic marker.

Estimation of the novel gene signature for independent prognostic prediction in training and validation sets. To further validate the efficacy of the risk score in the prognostic prediction of patients with LUAD, TCGA-LUAD cohort (training set) was divided into two groups according to the median value of the risk score. The patients in the high-risk score group had a shorter survival time and an increased ratio of 'DEAD' status compared with the patients in the low-risk score group (Fig. 4A). The same results were illustrated in the two independent validation sets, GSE30219 and GSE31210, obtained from the GEO database (Fig. 4B and C). Heatmaps of the 18 genes in the training set and validation sets are presented in Fig. 4D-F.

Furthermore, Kaplan-Meier plots were used to examine the ability of the novel signature to predict prognosis. As presented

in Fig. 5A-C, an increased probability of a longer survival time was positively correlated with a low-risk score of the novel gene signature in the training set and the two validation sets.

Correlation between the novel gene signature and tumor-infiltrating immune cells. Tumor cells interact with tumor-infiltrating immune cells such as macrophages to induce the immunoinhibitory phenotype (22,23). Considering that these genes were endocytosis-associated genes, the present study attempted to investigate the association between the novel signature and tumor-infiltrating immune cells of LUAD. The ESTIMATE algorithm was used to calculate tumor purity scores, and these were compared with the risk scores of the novel signature in TCGA-LUAD cohort. As presented in Fig. 6A-C, the risk score was negatively correlated with the stromal and immune scores, but positively correlated with tumor purity, indicating that patients with a low-risk score had a more complicated immune microenvironment. Immune cell compositions in different groups with high or low risk scores were further examined using the CIBERSORTx algorithm. B cells, plasma cells, CD4^{+} T cells, monocytes, dendritic and mast cells had an increased
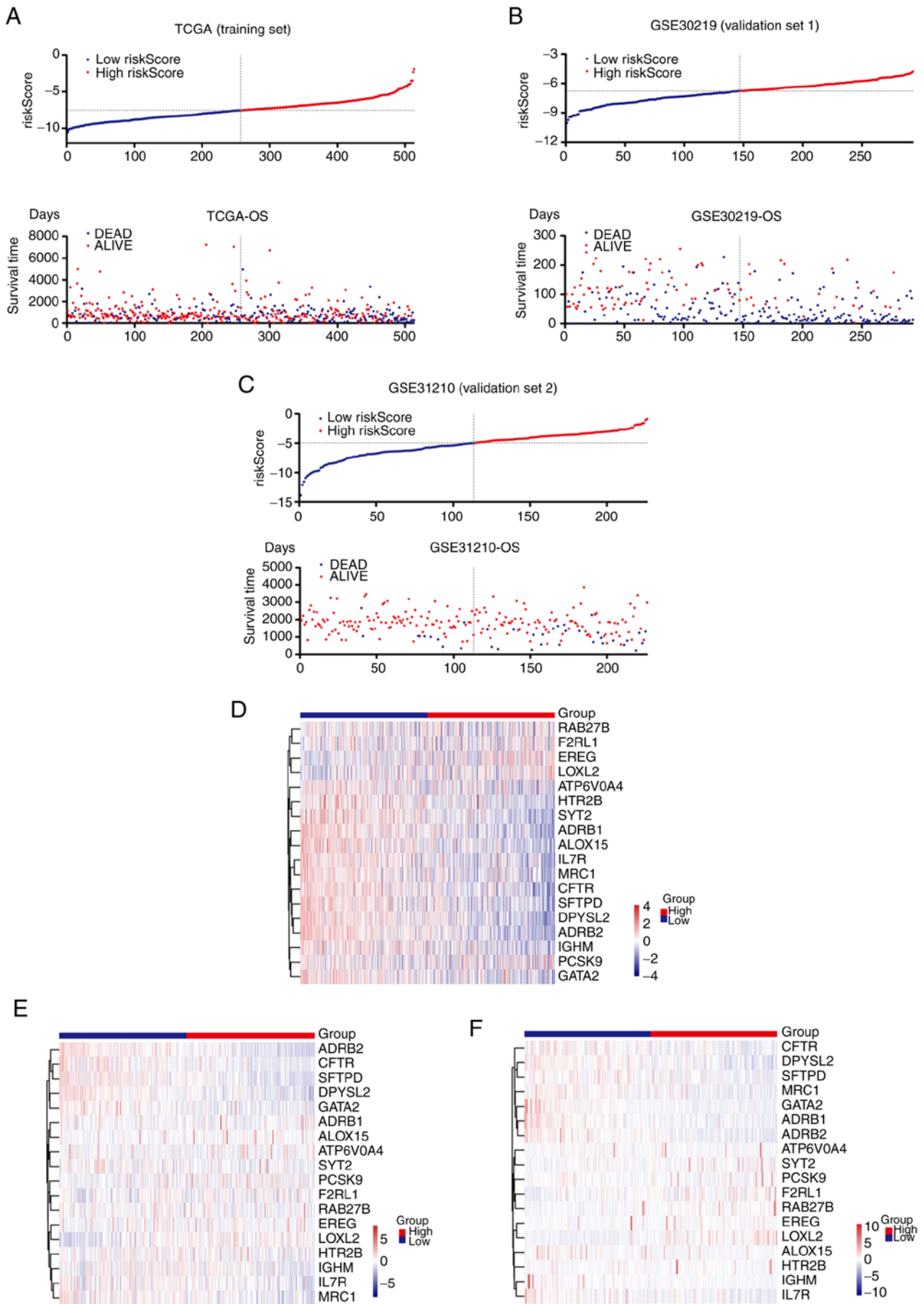
Figure 4. Correlation between risk score and survival outcome in TCGA-LUAD and Gene Expression Omnibus cohorts. Scatter plots present the distribution of the risk score and survival status of patients in (A) TCGA-LUAD, (B) GSE30219 and (C) GSE31210 cohorts. Heatmaps of the genes in the novel signature in (D) TCGA-LUAD, (E) GSE30219 and (F) GSE31210 cohorts. TCGA, The Cancer Genome Atlas; LUAD, lung adenocarcinoma; OS, overall survival.
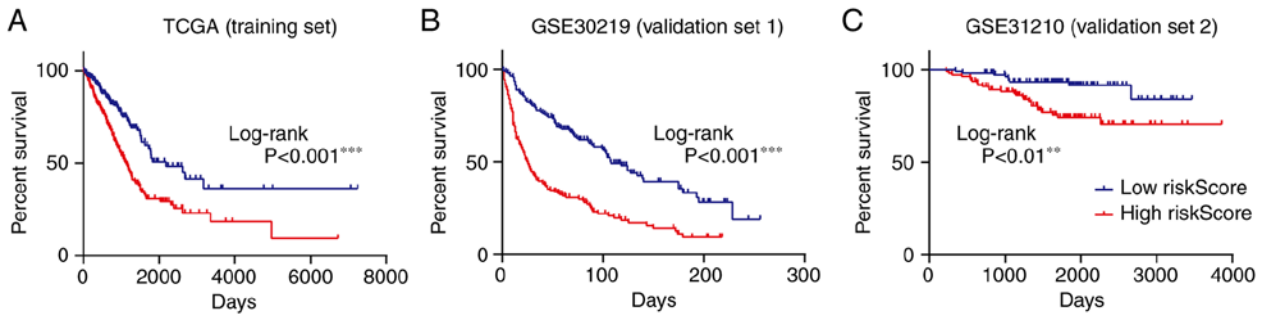
Figure 5. Overall survival analysis in high- and low-risk scores from TCGA-LUAD and Gene Expression Omnibus cohorts. Kaplan-Meier curves of the risk score in (A) TCGA-LUAD, (B) GSE30219 and (C) GSE31210 cohorts. **P<0.01; ***P<0.001. TCGA, The Cancer Genome Atlas; LUAD, lung adenocarcinoma.
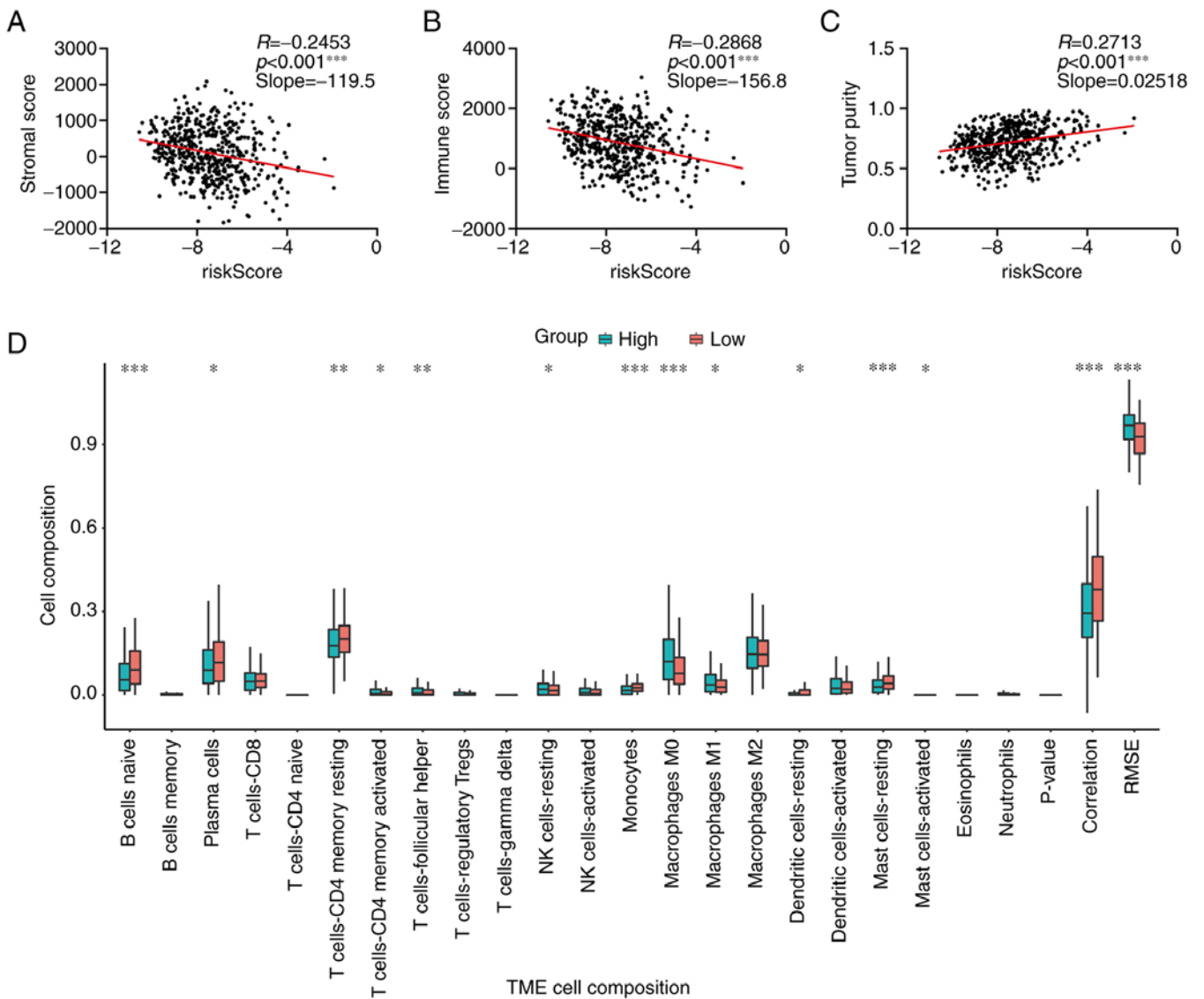

Figure 6. Correlation between risk score and immune microenvironment of LUAD. The risk scores of patients in the LUAD cohort from The Cancer Genome Atlas database were negatively correlated with (A) stromal score and (B) immune score, but were positively correlated with (C) tumor purity using Pearson's correlation coefficient. (D) Box plots depicting the distributions of risk scores in different immune cell compositions. *P<0.05; **P<0.01; ***P<0.001. LUAD, lung adenocarcinoma; TME, tumor microenvironment; RMSE, root mean square error.

composition in the low-risk score group compared with the high-risk score group; however, the NK cells and M0 and M1 macrophages were increased in the high-risk score group compared with the low-risk score group (Fig. 6D). In

addition, the correlation between the risk score and marker genes of different immune cells was calculated. As presented in Table II, the majority of genes were negatively associated with these genes. These findings indicated that the novel gene

Table II. Correlation analysis between riskScore and marker genes of immune cells in The Cancer Genome Atlas-lung adeno-carcinoma cohort.

Immune cell	Marker gene	Correlation	P-value
T cell	CD3G	-0.372	1.19×10^{-16}[a]
	CD3D	-0.296	2.80×10^{-10}[a]
	CD3E	-0.362	1.05×10^{-15}[a]
	CD2	-0.362	1.17×10^{-15}[a]
Monocyte	CD86	-0.342	6.57×10^{-14}[a]
	CSF1R	-0.393	1.08×10^{-18}[a]
Tumor-associated macrophage	CCL2	-0.211	4.02×10^{-5}[a]
	CD68	-0.233	3.13×10^{-6}[a]
	IL10	-0.338	1.44×10^{-13}[a]
M1 macrophage	INOS	-0.200	1.34×10^{-4}[a]
	IRF5	-0.255	1.53×10^{-7}[a]
	COX2	-0.109	2.80×10^{-1}[b]
M2 macrophage	CD163	-0.314	1.41×10^{-11}[a]
	VSIG4	-0.308	3.88×10^{-11}[a]
	MS4A4A	-0.355	4.68×10^{-15}[a]
	MRC1	-0.439	6.14×10^{-24}[a]
Dendritic cell	HLA-DPB1	-0.492	4.07×10^{-31}[a]
	HLA-DQB1	-0.414	5.30×10^{-21}[a]
	HLA-DRA	-0.442	2.83×10^{-24}[a]
	CD1C	-0.531	3.13×10^{-37}[a]
	NRP1	-0.238	1.58×10^{-6}[a]
	ITGAX	-0.424	3.25×10^{-22}[a]
Regulatory T cell	FOXP3	-0.295	3.52×10^{-10}[a]
	CCR8	-0.315	1.16×10^{-11}[a]
	STAT5B	-0.406	3.50×10^{-20}[a]
	TGFB1	-0.247	4.66×10^{-7}[a]
T cell exhaustion	PD-1	-0.196	2.00×10^{-4}[a]
	CTLA4	-0.315	1.24×10^{-11}[a]
	LAG3	-0.151	1.40×10^{-2}[c]
	TIM-3	-0.303	9.39×10^{-11}[a]
	GZMB	0.027	5.41×10^{-1}[b]

[a]$P<0.001$; [b]$P \geq 0.05$; [c]$P<0.05$. Pearson's correlation coefficient was determined.

signature could hint at the complexity of the tumor microenvironment.

Inhibition of endocytosis by CQ reduced proliferation and increased apoptosis in lung cancer. To further investigate the expression levels of endocytosis-associated genes in the novel signature, total RNA was isolated from the lung epithelial cell line BEAS-2B and the lung cancer cell lines A549, H1975, H1299 and PC9, and then reverse transcribed for qPCR assays. The result was visualized as a heatmap in Fig. 7A. Compared with the levels in BEAS-2B cells, the expression levels of RAB27B, ATP6V0A4, LOXL2, HTR2B, SYT2, F2RL1 and IGHM were increased in lung cancer cells, and the other genes had decreased expression levels in tumor cells, which was consistent with the expression patterns in TCGA-LUAD dataset (Fig. 2D).

CQ is a conventional drug for treating amebiasis. CQ has been reported to induce a blockade of endocytosis via pH changes in lysosomes in cells (24). Given the roles of endocytosis in LUAD progression and the value of the endocytosis-associated signature in the prognostic prediction of patients with LUAD, CQ was used to treat lung cancer cell lines as well as normal lung epithelial cell lines. CQ treatment decreased the expression levels of the genes that were positively correlated with poor prognosis, and increased the expression levels of genes that were negatively associated with short survival time in lung cancer cells such as A549, H1299, H1975 and PC9 (Fig. 7B). However, the CQ-induced expression level changes in these genes were not consistently observed in BEAS-2B (Fig. 7B), indicating that CQ had a preferential effect on tumor cells. In addition, CQ treatment decreased the viability of A549, H1975, H1299 and PC9 cells, but no such effect was observed in BEAS-2B cells (Fig. 8A). EdU staining indicated reduced proliferation of lung cancer cell lines in the CQ treatment group compared with that in
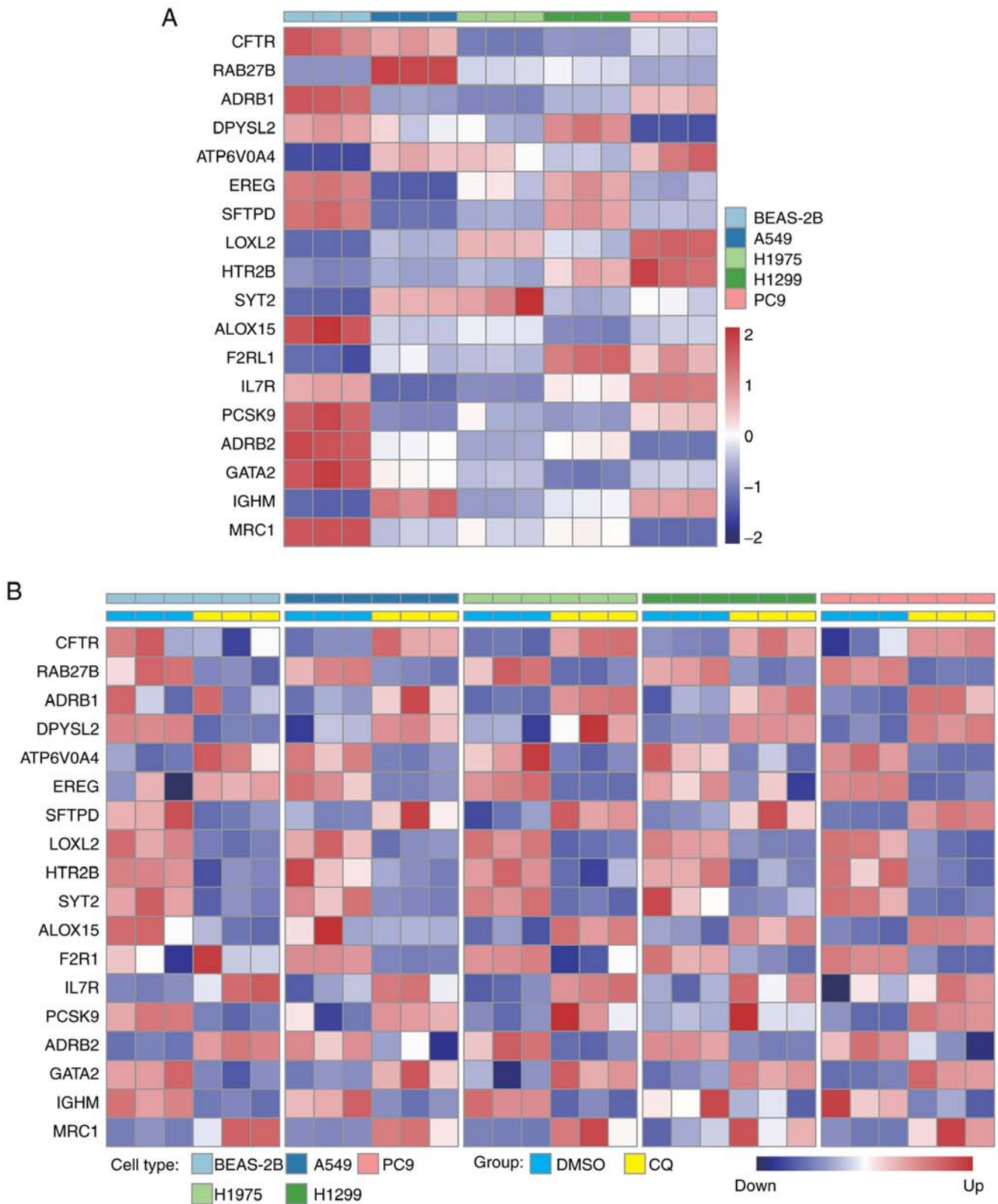
Figure 7. CQ treatment altered the expression profiles of signature genes. (A) Relative expression levels of CFTR, RAB27B, ADRB1, DPYSL2, ATP6V0A4, EREG, SFTPD, LOXL2, HTR2B, SYT2, ALOX15, F2RL1, IL7R, PCSK9, ADRB2, GATA2, IGHM and MRC1 in BEAS-2B, A549, H1975, H1299 and PC9 cells. (B) Relative expression levels of the aforementioned genes were detected after CQ treatment. CQ, chloroquine.

the DMSO group (Fig. 8B). Additionally, the level of apoptosis after stimulation with CQ was examined in these cells. Flow cytometry results revealed that the percentage of apoptotic cells was increased, and that of live cells was decreased after CQ treatment (Fig. 9). Taken together, these results suggest that CQ treatment resulted in an inhibited proliferation and increased apoptosis of lung cancer cells, presumably due to the reversal of gene expression patterns in tumors, demonstrating that targeting
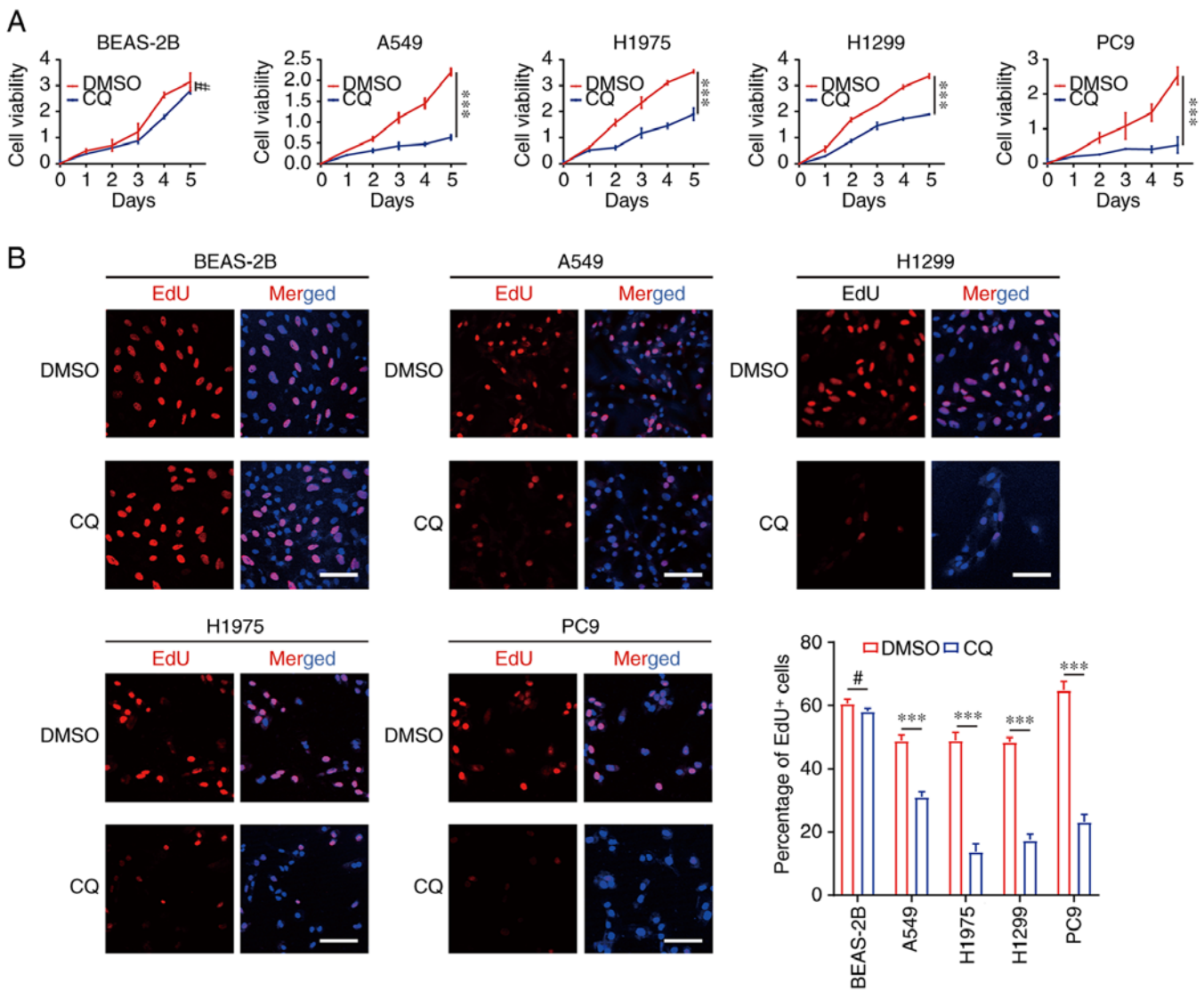
Figure 8. CQ treatment decreased lung cancer cell proliferation. (A) Cell viabilities of BEAS-2B, A549, H1975, H1299 and PC9 cells upon CQ treatment were measured using the Cell Counting Kit-8 assay. (B) EdU staining of BEAS-2B, A549, H1975, H1299 and PC9 cells stimulated with CQ was imaged using confocal microscopy. Statistical analysis of EdU positive cells was performed using ImageJ (version 1.53; National Institutes of Health). [#]P>0.05; [***]P<0.001. Scale bar, 100 μM. CQ, chloroquine.

endocytosis could benefit the clinical treatment of patients with lung cancer, including patients with a high-risk score.

Discussion

Endocytosis is one of the essential functions of cell biology and serves an extensive role in the development of tumors (25). Uptake and excretion are mediated by endocytosis and exocytosis maintains the integrity and kinetics of the cell membrane, supporting the rapid proliferation of tumor cells (26). Furthermore, endocytosis can seize the majority of nutrients from the surroundings to promote energy metabolism and lead to nutrient deficiency of ambient stromal cells and infiltrated immune cells, thus regulating the immunosuppressive microenvironment construction (27). In the present study, the focus was on an endocytosis-associated gene set used to screen candidate genes that not only promote the malignant progression of LUAD, but are also associated with a poor prognosis. Subsequently, a novel prognostic gene signature

consisting of 18 genes was further refined and established, and the association between this signature and tumor grade and stage was examined. Finally, it was also confirmed that a high score of the gene signature was positively correlated with lower tumor purity and more complex immune cell infiltration. Since no endocytosis-associated gene signature has been reported in LUAD for prognosis prediction, the findings of the present study are expected to further confirm the key roles of endocytosis in tumorigenesis, and provide a powerful strategy for early diagnosis and prognosis determination of LUAD.

Receptor tyrosine kinases (RTKs) are a type of transmembrane protein that transduce stimulatory signals to downstream proteins in a ligand-dependent manner (28). Aberrant activation of the RTK pathway usually occurs in tumorigenesis and malignant progression (29). EGFR is an important RTK, and its oncogenic mutation accounts for ~20% of patients with LUAD (30). TKIs target kinase receptors, such as EGFR, fibroblast growth factor receptor, platelet-derived growth factor receptor and vascular endothelial growth factor receptor,
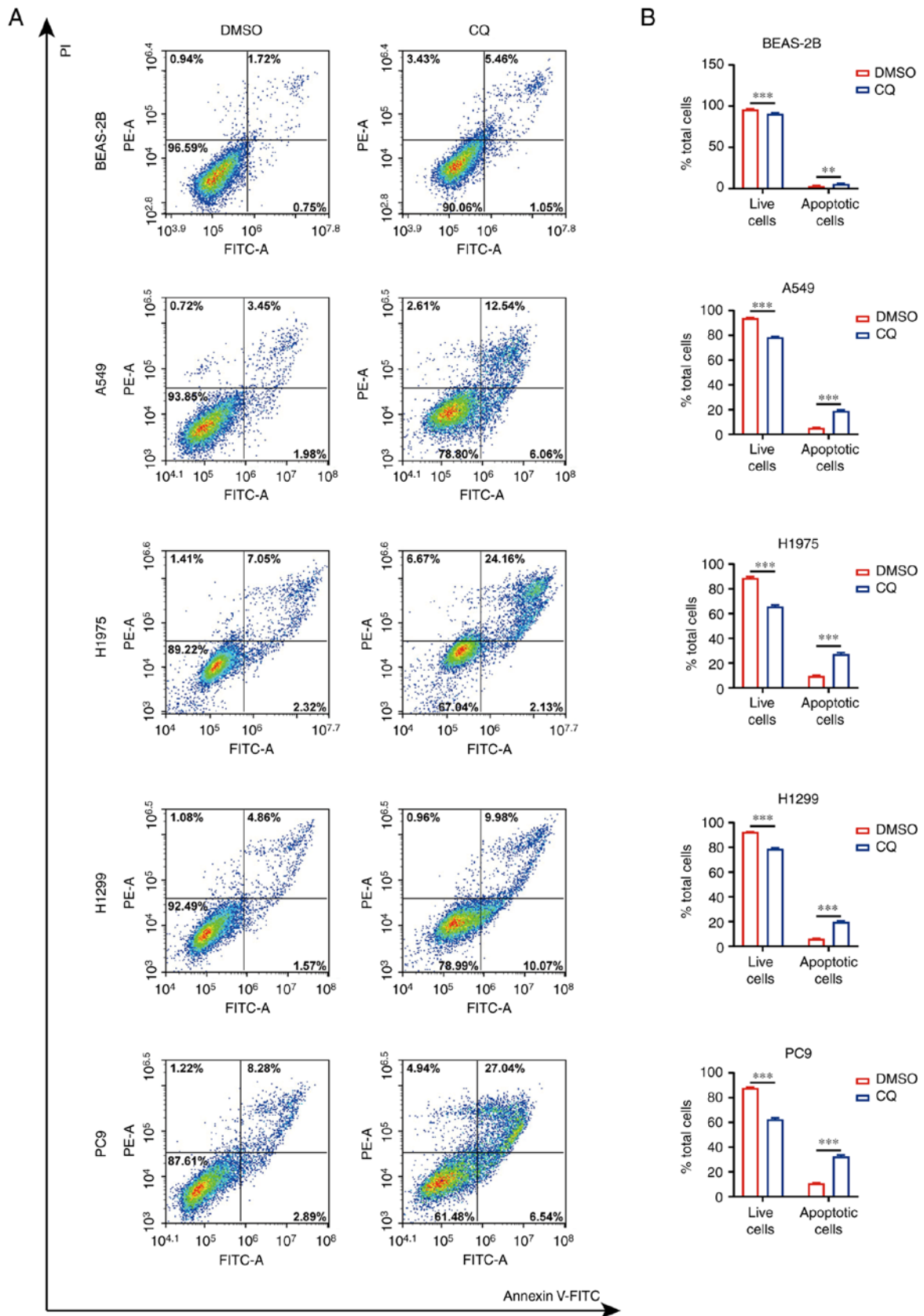
Figure 9. CQ treatment increased apoptosis of lung cancer cells. (A) Scatter plots demonstrating the distributions of live and apoptotic cells after CQ treatment in BEAS-2B, A549, H1975, H1299 and PC9 cells. (B) Quantification of the results of flow cytometry. $^{**}P<0.01$; $^{***}P<0.001$. CQ, chloroquine.

which block activation of the downstream cascade. Currently, first-generation (gefitinib and erlotinib), second-generation (afatinib) and third-generation (osimertinib) TKIs have been approved for clinical LUAD treatment (31-33). A number of patients can benefit from TKI treatment, while others will still suffer from recurrence (34). It has been reported that

internalization of EGFR mediated by endocytosis is one of the direct reasons for TKI treatment failure (35). In addition, tumors can also become drug resistant through a bypass activation mechanism, leading to poor prognosis (36). The findings of the present study classified patients with LUAD using an endocytosis-associated signature. CQ treatment could reduce the proliferation of lung cancer cells. Considering the correlation between endocytosis and RTK activation, the combined treatment strategy of TKIs and endocytosis blockers is expected to result in a better prognosis for patients with high-score LUAD.

In recent years, tumor immunotherapy has demonstrated strong antitumor effects, but a number of patients have developed drug resistance to this therapy (37). Chew *et al* (38) revealed that inhibition of endocytosis can effectively improve the killing effect of monoclonal antibodies against tumor immunotherapy. Through retrospective analysis, it was confirmed that the score based on the endocytosis-associated signature was correlated with immune infiltration. Therefore, patients with high scores might benefit from improved therapeutic effects through treatment with immunotherapy affiliated with endocytosis inhibitors.

Currently, various studies have explored prognostic prediction of lung cancer from different perspectives, the majority of which focus on the area of tumor immunity. Sun *et al* (39) established a long non-coding RNA signature associated with the immune infiltration of LUAD. Another study identified 10 genes associated with immune infiltration and constructed a prediction model for SCLC (40). Li *et al* (41) integrated multiple cohorts to develop and validate an immune signature composed of 25 genes predicting early-stage NSCLC. A study used Lasso Cox regression analysis to identify four immune-associated gene signatures that could adequately predict the prognosis of patients with LUAD (42). In addition, a number of studies have also established models for crucial biological processes of tumors, such as anoikic (43) and glycolysis (44), which were reported to be associated with the prognosis of patients. In the present study, a univariate/multivariate Cox regression analysis combined with Lasso Cox regression analysis was used to identify 18 genes that were significantly associated with patient outcomes, and a novel signature in terms of tumor endocytosis was established. Subsequently, treatment with the endocytosis inhibitor CQ significantly inhibited proliferation, and increased apoptosis levels of LUAD cells. The present study not only provided a prognostic prediction model for clinical patients with LUAD, but also an alternative treatment for patients with high scores.

In the present study, the novel endocytosis-associated gene signature established by the LUAD cohort of TCGA database and verified by two GEO datasets included the following 18 genes: CFTR, RAB27B, ADRB1, DPYSL2, ATP6V0A4, EREG, SFTPD, LOXL2, HTR2B, SYT2, ALOX15, F2R1, IL7R, PCSK9, ADRB2, GATA2, IGMH and MRC1. Considering that these genes belong to the gene set of endocytosis, a number of them are membrane localization proteins, including CFTR, ADRB1, ATP6V0A4, EREG, SFTPD, HTR2B, ALOX15, F2RL1, IL7R, ADRB2, IGMH and MRC1. Notably, the functional importance of a number of the genes in LUAD has been reported. CFTR mutations

are closely associated with cystic fibrosis and tumorigenesis of lung cancer (45,46). EREG induces EGFR/ErbB2 heterodimer formation to phosphorylate AKT and block TKI-mediated apoptosis in NSCLC (47), whereas SFTPD inhibits the dimerization and activation of EGFR (48). LOXL2 induced by the microRNA-200/ZEB1 axis mediates extracellular matrix reprogramming to promote the invasion and metastasis of lung cancer (49). IL7R not only activates the JAK/STAT5 signaling pathway to sensitize NSCLC to chemotherapeutics (50), but also acts as a transmitter for IL-7-induced sensitization to cisplatin by activating the PI3K/AKT pathway and enhancing ABCG2 expression (51). GATA2 was proven to be essential for RAS-driven NSCLC (52). The expression levels of RAB27B (53), DPYSL2 (54), ALOX15 (55) and PCSK9 (56) were reported to be closely associated with the prognosis of patients with lung cancer. In addition, the functional roles of HTR2B, F2RL1 and SYT2 in lung cancer remain unclear, suggesting that a number of mechanisms require further investigation.

The present study has certain limitations which need to be carefully addressed. The endocytosis-associated signature established was based on data from TCGA and two other cohorts originating from RNA sequencing. The expression profiles of signature genes under the treatment of CQ were validated by qPCR in LUAD cell lines. However, the levels of proteins involved in this signature remained unclear after CQ treatment, and a number of proteins might serve important roles in malignant behavior of lung cancer, the mechanism of which requires further investigation. In addition, it is hypothesized that if verified using a larger dataset, a PCR-based diagnostic kit according to this signature could be developed for accurate prognostic prediction of patients with LUAD.

In conclusion, a novel endocytosis-associated prognostic signature was depicted using TCGA and GEO datasets. High risk scores of patients with LUAD, calculated according to the signature, indicated poor prognosis and short survival time. The gene signature helped to identify the immunosuppressive tumor microenvironment, suggesting that anti-endocytosis therapy could significantly improve the prognosis of patients with LUAD. Additionally, targeting endocytosis via CQ could repress tumor proliferation *in vitro*. Based on the aforementioned findings, personalized diagnosis and targeted combinational therapeutic strategies for patients with LUAD could be provided.

Availability of data and materials

TCGA data used in the present study were downloaded from the UCSC Xena online server (https://xenabrowser.net/). The GSE30219 and GSE31210 datasets were downloaded from the GEO database (https://www.ncbi.nlm.nih.gov/geo/).

Authors' contributions

YiZ, ML and KZ conceptualized and designed the study. YiZ, SL, YaZ and ML carried out the experiments. YiZ and SL analyzed the data and generated the figures. YiZ, ML and KZ drafted the manuscript. ML and KZ confirm the authenticity of all the raw data. All authors read and approved the final version of the manuscript.

Ethics approval and consent to participate

Not applicable.

Patient consent for publication

Not applicable.

Competing interests

The authors declare that they have no competing interests.

References

1. Nasim F, Sabath BF and Eapen GA: Lung cancer. Med Clin North Am 103: 463-473, 2019.
2. Li C, Lei S, Ding L, Xu Y, Wu X, Wang H, Zhang Z, Gao T, Zhang Y and Li L: Global burden and trends of lung cancer incidence and mortality. Chin Med J (Engl) 136: 1583-1590, 2023.
3. Detterbeck FC, Boffa DJ, Kim AW and Tanoue LT: The eighth edition lung cancer stage classification. Chest 151: 193-203, 2017.
4. Herbst RS, Morgensztern D and Boshoff C: The biology and management of non-small cell lung cancer. Nature 553: 446-454, 2018.
5. Duma N, Santana-Davila R and Molina JR: Non-small cell lung cancer: epidemiology, screening, diagnosis, and treatment. Mayo Clin Proc 94: 1623-1640, 2019.
6. Hirsch FR, Scagliotti GV, Mulshine JL, Kwon R, Curran WJ Jr, Wu YL and Paz-Ares L: Lung cancer: Current therapies and new targeted treatments. Lancet 389: 299-311, 2017.
7. Doherty GJ and McMahon HT: Mechanisms of endocytosis. Annu Rev Biochem 78: 857-902, 2009.
8. Lanzetti L and Di Fiore PP: Endocytosis and cancer: An 'insider' network with dangerous liaisons. Traffic 9: 2011-2021, 2008.
9. Théry C, Ostrowski M and Segura E: Membrane vesicles as conveyors of immune responses. Nat Rev Immunol 9: 581-593, 2009.
10. Chen PH, Bendris N, Hsiao YJ, Reis CR, Mettlen M, Chen HY, Yu SL and Schmid SL: Crosstalk between CLCb/Dyn1-mediated adaptive clathrin-mediated endocytosis and epidermal growth factor receptor signaling increases metastasis. Dev Cell 40: 278-288.e5, 2017.
11. Ketteler J and Klein D: Caveolin-1, cancer and therapy resistance. Int J Cancer 143: 2092-2104, 2018.
12. Roy S, Wyse B and Hancock JF: H-Ras signaling and K-Ras signaling are differentially dependent on endocytosis. Mol Cell Biol 22: 5128-5140, 2002.
13. Kim B, Park YS, Sung JS, Lee JW, Lee SB and Kim YH: Clathrin-mediated EGFR endocytosis as a potential therapeutic strategy for overcoming primary resistance of EGFR TKI in wild-type EGFR non-small cell lung cancer. Cancer Med 10: 372-385, 2021.
14. Xiao GY, Mohanakrishnan A and Schmid SL: Role for ERK1/2-dependent activation of FCHSD2 in cancer cell-selective regulation of clathrin-mediated endocytosis. Proc Natl Acad Sci USA 115: E9570-E9579, 2018.
15. Jo U, Park KH, Whang YM, Sung JS, Won NH, Park JK and Kim YH: EGFR endocytosis is a novel therapeutic target in lung cancer with wild-type EGFR. Oncotarget 5: 1265-1278, 2014.
16. Nishimura Y, Bereczky B and Ono M: The EGFR inhibitor gefitinib suppresses ligand-stimulated endocytosis of EGFR via the early/late endocytic pathway in non-small cell lung cancer cell lines. Histochem Cell Biol 127: 541-553, 2007.
17. Nishimura Y, Yoshioka K, Bereczky B and Itoh K: Evidence for efficient phosphorylation of EGFR and rapid endocytosis of phosphorylated EGFR via the early/late endocytic pathway in a gefitinib-sensitive non-small cell lung cancer cell line. Mol Cancer 7: 42, 2008.
18. Tanaka T, Ozawa T, Oga E, Muraguchi A and Sakurai H: Cisplatin-induced non-canonical endocytosis of EGFR via p38 phosphorylation of the C-terminal region containing Ser-1015 in non-small cell lung cancer cells. Oncol Lett 15: 9251-9256, 2018.
19. Love MI, Huber W and Anders S: Moderated estimation of fold change and dispersion for RNA-seq data with DESeq2. Genome Biol 15: 550, 2014.
20. Yoshihara K, Shahmoradgoli M, Martinez E, Vegesna R, Kim H, Torres-Garcia W, Treviño V, Shen H, Laird PW, Levine DA, et al: Inferring tumour purity and stromal and immune cell admixture from expression data. Nat Commun 4: 2612, 2013.
21. Livak KJ and Schmittgen TD: Analysis of relative gene expression data using real-time quantitative PCR and the 2(-Delta Delta C(T)) method. Methods 25: 402-408, 2001.
22. Park JV, Chandra R, Cai L, Ganguly D, Li H, Toombs JE, Girard L, Brekken RA and Minna JD: Tumor cells modulate macrophage phenotype in a novel in vitro co-culture model of the NSCLC tumor microenvironment. J Thorac Oncol 17: 1178-1191, 2022.
23. Park JE, Dutta B, Tse SW, Gupta N, Tan CF, Low JK, Yeoh KW, Kon OL, Tam JP and Sze SK: Hypoxia-induced tumor exosomes promote M2-like macrophage polarization of infiltrating myeloid cells and microRNA-mediated metabolic shift. Oncogene 38: 5158-5173, 2019.
24. Tripathy S, Dassarma B, Roy S, Chabalala H and Matsabisa MG: A review on possible modes of action of chloroquine/hydroxychloroquine: Repurposing against SAR-CoV-2 (COVID-19) pandemic. Int J Antimicrob Agents 56: 106028, 2020.
25. Johannes L and Billet A: Glycosylation and raft endocytosis in cancer. Cancer Metastasis Rev 39: 375-396, 2020.
26. Cooper ST and McNeil PL: Membrane repair: Mechanisms and pathophysiology. Physiol Rev 95: 1205-1240, 2015.
27. Xiao Y, Rabien A, Buschow R, Amtislavskiy V, Busch J, Kilic E, Villegas SL, Timmermann B, Schütte M, Mielke T, et al: Endocytosis-mediated replenishment of amino acids favors cancer cell proliferation and survival in chromophobe renal cell carcinoma. Cancer Res 80: 5491-5501, 2020.
28. Azad T, Rezaei R, Surendran A, Singaravelu R, Boulton S, Dave J, Bell JC and Ilkow CS: Hippo signaling pathway as a central mediator of receptors tyrosine kinases (RTKs) in tumorigenesis. Cancers (Basel) 12: 2042, 2020.
29. Du Z and Lovly CM: Mechanisms of receptor tyrosine kinase activation in cancer. Mol Cancer 17: 58, 2018.
30. da Cunha Santos G, Shepherd FA and Tsao MS: EGFR mutations and lung cancer. Annu Rev Pathol 6: 49-69, 2011.
31. Sim EH, Yang IA, Wood-Baker R, Bowman RV and Fong KM: Gefitinib for advanced non-small cell lung cancer. Cochrane Database Syst Rev 1: CD006847, 2018.
32. Sartori G, Belluomini L, Lombardo F, Avancini A, Trestini I, Vita E, Tregnago D, Menis J, Bria E, Milella M and Pilotto S: Efficacy and safety of afatinib for non-small-cell lung cancer: State-of-the-art and future perspectives. Expert Rev Anticancer Ther 20: 531-542, 2020.
33. Remon J, Steuer CE, Ramalingam SS and Felip E: Osimertinib and other third-generation EGFR TKI in EGFR-mutant NSCLC patients. Ann Oncol 29 (Suppl 1): i20-i27, 2018.
34. Wu SG and Shih JY: Management of acquired resistance to EGFR TKI-targeted therapy in advanced non-small cell lung cancer. Mol Cancer 17: 38, 2018.
35. Cruz Da Silva E, Choulier L, Thevenard-Devy J, Schneider C, Carl P, Ronde P, Dedieu S and Lehmann M: Role of endocytosis proteins in gefitinib-mediated EGFR internalisation in glioma cells. Cells 10: 3258, 2021.
36. McCoach CE, Le AT, Gowan K, Jones K, Schubert L, Doak A, Estrada-Bernal A, Davies KD, Merrick DT, Bunn PA Jr, et al: Resistance mechanisms to targeted therapies in ROS1+ and ALK+ non-small cell lung cancer. Clin Cancer Res 24: 3334-3347, 2018.
37. Mamdani H, Matosevic S, Khalid AB, Durm G and Jalal SI: Immunotherapy in lung cancer: Current landscape and future directions. Front Immunol 13: 823618, 2022.
38. Chew HY, De Lima PO, Gonzalez Cruz JL, Banushi B, Echejoh G, Hu L, Joseph SR, Lum B, Rae J, O'Donnell JS, et al: Endocytosis inhibition in humans to improve responses to ADCC-mediating antibodies. Cell 180: 895-914.e27, 2020.

39. Sun J, Zhang Z, Bao S, Yan C, Hou P, Wu N, Su J, Xu L and Zhou M: Identification of tumor immune infiltration-associated lncRNAs for improving prognosis and immunotherapy response of patients with non-small cell lung cancer. J Immunother Cancer 8: e000110, 2020.

40. Xie Q, Chu H, Yi J, Yu H, Gu T, Guan Y, Liu X, Liang J, Li Y and Wang J: Identification of a prognostic immune-related signature for small cell lung cancer. Cancer Med 10: 9115-9128, 2021.

41. Li B, Cui Y, Diehn M and Li R: Development and validation of an individualized immune prognostic signature in early-stage nonsquamous non-small cell lung cancer. JAMA Oncol 3: 1529-1537, 2017.

42. Sun S, Guo W, Wang Z, Wang X, Zhang G, Zhang H, Li R, Gao Y, Qiu B, Tan F, *et al*: Development and validation of an immune-related prognostic signature in lung adenocarcinoma. Cancer Med 9: 5960-5975, 2020.

43. Diao X, Guo C and Li S: Identification of a novel anoikis-related gene signature to predict prognosis and tumor microenvironment in lung adenocarcinoma. Thorac Cancer 14: 320-330, 2023.

44. Zhang L, Zhang Z and Yu Z: Identification of a novel glycolysis-related gene signature for predicting metastasis and survival in patients with lung adenocarcinoma. J Transl Med 17: 423, 2019.

45. Govindan R, Ding L, Griffith M, Subramanian J, Dees ND, Kanchi KL, Maher CA, Fulton R, Fulton L, Wallis J, *et al*: Genomic landscape of non-small cell lung cancer in smokers and never-smokers. Cell 150: 1121-1134, 2012.

46. Shi X, Kou M, Dong X, Zhai J, Liu X, Lu D, Ni Z, Jiang J and Cai K: Integrative pan cancer analysis reveals the importance of CFTR in lung adenocarcinoma prognosis. Genomics 114: 110279, 2022.

47. Ma S, Zhang L, Ren Y, Dai W, Chen T, Luo L, Zeng J, Mi K, Lang J and Cao B: Epiregulin confers EGFR-TKI resistance via EGFR/ErbB2 heterodimer in non-small cell lung cancer. Oncogene 40: 2596-2609, 2021.

48. Umeda Y, Hasegawa Y, Otsuka M, Ariki S, Takamiya R, Saito A, Uehara Y, Saijo H, Kuronuma K, Chiba H, *et al*: Surfactant protein D inhibits activation of non-small cell lung cancer-associated mutant EGFR and affects clinical outcomes of patients. Oncogene 36: 6432-6445, 2017.

49. Peng DH, Ungewiss C, Tong P, Byers LA, Wang J, Canales JR, Villalobos PA, Uraoka N, Mino B, Behrens C, *et al*: ZEB1 induces LOXL2-mediated collagen stabilization and deposition in the extracellular matrix to drive lung cancer invasion and metastasis. Oncogene 36: 1925-1938, 2017.

50. Shi L, Xu Z, Yang Q, Huang Y, Gong Y, Wang F and Ke B: IL-7-Mediated IL-7R-JAK3/STAT5 signalling pathway contributes to chemotherapeutic sensitivity in non-small-cell lung cancer. Cell Prolif 52: e12699, 2019.

51. Ke B, Wei T, Huang Y, Gong Y, Wu G, Liu J, Chen X and Shi L: Interleukin-7 resensitizes non-small-cell lung cancer to cisplatin via inhibition of ABCG2. Mediators Inflamm 2019: 7241418, 2019.

52. Kumar MS, Hancock DC, Molina-Arcas M, Steckel M, East P, Diefenbacher M, Armenteros-Monterroso E, Lassailly F, Matthews N, Nye E, *et al*: The GATA2 transcriptional network is requisite for RAS oncogene-driven non-small cell lung cancer. Cell 149: 642-655, 2012.

53. Koh HM and Song DH: Prognostic role of Rab27A and Rab27B expression in patients with non-small cell lung carcinoma. Thorac Cancer 10: 143-149, 2019.

54. Wu YJ, Nai AT, He GC, Xiao F, Li ZM, Tang SY, Liu YP and Ai XH: DPYSL2 as potential diagnostic and prognostic biomarker linked to immune infiltration in lung adenocarcinoma. World J Surg Oncol 19: 274, 2021.

55. Ren Z, Hu M, Wang Z, Ge J, Zhou X, Zhang G and Zheng H: Ferroptosis-related genes in lung adenocarcinoma: Prognostic signature and immune, drug resistance, mutation analysis. Front Genet 12: 672904, 2021.

56. Xie M, Yu X, Chu X, Xie H, Zhou J, Zhao J and Su C: Low baseline plasma PCSK9 level is associated with good clinical outcomes of immune checkpoint inhibitors in advanced non-small cell lung cancer. Thorac Cancer 13: 353-360, 2022.